Available online at www.sciencedirect.com

ScienceDirect

International Journal of Heat and Mass Transfer 50 (2007) 2376–2393

International Journal of HEAT and MASS TRANSFER

www.elsevier.com/locate/ijhmt

Convective mass transfer coefficient for a hydrodynamically developed airflow in a short rectangular duct

Conrad R. Iskra, Carey J. Simonson *

Department of Mechanical Engineering, University of Saskatchewan, 57 Campus Drive, Saskatoon, Sask., Canada S7N 5A9

Received 31 March 2006; received in revised form 21 October 2006
Available online 18 December 2006

Abstract

In this paper, experiments are performed to determine the convective mass transfer coefficient for evaporation in a horizontal rectangular duct with an aspect ratio of 14.5:1. In the test facility, a short pan of water forms the lower panel of a long duct where a hydrodynamically fully developed laminar or turbulent airflow passes over the surface of the water. The measured convective mass transfer coefficients have uncertainties that are typically less than ±10% and are presented for Reynolds numbers (*Re*) between 570 and 8100, Rayleigh numbers (*Ra*) between 6300 and 83,000, inverse Graetz numbers (*Gz*) between 0.003 and 0.04, and operating conditions factors (H^*) between −3.6 and −1.4. The measured convective mass transfer coefficients are found to increase as *Re*, *Ra*, *Gz* and H^* increase and these effects are included in the Sherwood number correlations presented in this paper, which summarize the experimental data.

Keywords: Convection; Rectangular duct; Experimental mass transfer; Evaporation; Sherwood; Rayleigh; Reynolds; Boundary layer

---

1. Introduction

The aim of this paper is to determine the convective mass transfer coefficient in a rectangular duct at varying Rayleigh and Reynolds numbers. The convective mass transfer coefficient is an important parameter, since it is a measure of the resistance to mass transfer between the fluid flowing in a duct and the surface of the duct. The convective coefficient depends on the hydrodynamic, thermal and concentration boundary layers and is an important parameter when studying moisture and contaminant transfer between flowing air and porous media [1–4], as well as condensation and frosting in heat exchangers [5–7]. Despite its importance, there are few experimental data available in the literature on convective mass transfer coefficients for ducts. In most cases, convective heat transfer coefficients have been measured and the analogy between heat and mass transfer is used to determine the convective mass transfer coefficient.

Chuck and Sparrow [8,9] performed an experiment where a rectangular pan of water was set into the bottom panel of a duct and turbulent air was passed through the duct and over the surface of the water. The thermal conditions of the air and water, and the evaporation rate were measured. The height of water in the pan was varied and two pan lengths of 12.5 and 27.9 cm were used. The convective mass transfer coefficient was determined and a correlation was developed for the Sherwood number, which served as an extrapolation formula for larger lengths of pans where $L/D_h \geqslant 23.8$ and $L/h \geqslant 18$ [8].

Prata and Sparrow [10] performed a similar experiment as Chuck and Sparrow [8], using a cylindrical container. The water level in the container was varied, and the resultant effect was measured and reported in the form of a Sherwood number for Reynolds numbers between 7300 and 48,600. It was found that the maximum Sherwood number occurred when the ratio of the step height of water from the top of the container to the diameter of the container was

---

[*] Corresponding author. Tel.: +1 306 966 5479; fax: +1 306 966 5427.
E-mail address: carey.simonson@usask.ca (C.J. Simonson).

0017-9310/$ - see front matter © 2006 Elsevier Ltd. All rights reserved.
doi:10.1016/j.ijheatmasstransfer.2006.10.026

Nomenclature

A_s	area of evaporating surface (m^2)
D	inside diameter of circular duct (m)
D_{AB}	binary mass diffusion coefficient (m^2/s)
D_h	hydraulic diameter of rectangular duct (m)
g	gravitational acceleration (m^2/s)
Gr_m	mass transfer Grashof number (Ra_D/Sc)
Gz	Graetz number
H	height of rectangular duct (m)
H^*	dimensionless operating condition factor that represents the ratio of latent to sensible energy differences between the air stream and the air in equilibrium with the water surface
h_{fg}	enthalpy of vaporization (J/kg)
h	average distance between the water surface and top of pan (m)
h_m	convective mass transfer coefficient (m/s)
k	thermal conductivity (W/m K)
L	length of water pan (m)
l	distance between the first and last static pressure tap immediately upstream of the test section (m)
$\dot{m}_{evap}$	evaporation rate of water (kg/s)
$\dot{m}$	mass flow rate of air (kg/s)
Nu_D	Nusselt number (based on the hydraulic diameter of the test section duct)
P	duct perimeter (m)
p	pressure (Pa)
Pr	Prandtl number
p_{sat}	saturated water vapour pressure (Pa)
Δp	pressure drop across the orifice plate (Pa)
r^2	correlation coefficient
Ra_D	Rayleigh number (based on the hydraulic diameter of the test section duct)
Ra_D^+	Rayleigh number (based on the definition given by [15])
Re_D	Reynolds number (based on the hydraulic diameter of the test section duct)
Re_u	Reynolds number (based on the hydraulic diameter of the duct immediately upstream of the test section)
RH	relative humidity
RTD	resistance temperature device
S^*	dimensionless parameter that represents the ratio between mass and heat transfer
Sc	Schmidt number
SEE	standard error estimate of a curve fit
Sh_D	Sherwood number (based on the hydraulic diameter of the test section duct)
T	temperature (K)
ΔT	temperature difference between the surface of the water and the air entering the test section (K)
TMT	transient moisture transfer
t	time (h)
t	Student t-value at a 95% confidence level
V	velocity of air within the duct immediately upstream of the test section (m/s)
V_{max}	maximum velocity of air within the duct immediately upstream of the test section (m/s)
W	width of duct (m)
ΔW	humidity ratio difference between the surface of the water and the air entering the test section (kg/kg)
w	width of water pan (m)
x	horizontal distance along the flow direction of the duct immediately upstream of the test section (m)
X^*	a dimensionless coordinate parallel to flow equivalent to Gz^{-1}
y	vertical distance from the bottom of the duct that is immediately upstream of the test section (m)

Greek symbols

γ	aspect ratio $= W/H$
ρ	density (kg/m^3)
μ	dynamic viscosity (Ns/m^2)
$\Delta\rho_v$	log-mean water vapour density difference (kg/m^3)
$\bar{\rho}$	mean mixture density of air (kg/m^3)
ϕ	relative humidity of the ambient air

Subscripts

1	bulk properties of air entering the test section
2	bulk properties of air leaving the test section
a	dry air properties
f	average properties in the boundary layer
g	moist air property including dry air and water vapour
i	is an index where $i = 1$ at the inlet and $i = 2$ at the outlet of the test section
∞	average properties across the test section
s	properties at the surface of the water
v	water vapour

0.5. The correlations of [8–10] accurately quantify mass transfer for the turbulent flow regime, but many applications in building science and environmental engineering have lower air velocities and therefore require mass transfer coefficients for laminar or natural convection airflow.

Pauken [11] performed experiments by evaporating heated water from a circular pan in a low speed wind tunnel. The evaporation boundary layer that resulted was a combined turbulent forced and turbulent free convection boundary layer, where the forced convection was dominated by the air velocity and the free convection was a result of the density difference between the air at the surface of the water and the ambient air. It was found that 30% of the evaporation rate was due to free convection when the ratio of Grashof number over the Reynolds number squared (Gr/Re^2) was 0.1. This study and others [12–14], demonstrate that natural convection is present in the evaporation boundary layer when the air speeds are low. These effects cannot be neglected in many building science and environmental problems such as moisture transfer between indoor air and porous building materials.

To further investigate the onset of convective instability for laminar forced convection in the thermal entrance region of horizontal ducts, a numerical study was performed by Lin et al. [15]. The top and two sidewalls of the duct were adiabatic, while the bottom wall had a thin heated water film with constant wall temperature and concentration. The temperature and concentration boundary layers were developing throughout the length of the duct, with a fully developed velocity profile set at the entrance of the duct. The effect of free convection on the local Sh_D was a result of combined thermal and mass diffusion effects and was quantified with an effective Rayleigh number (Ra_D^+). Results showed that an increase in Ra_D^+ resulted in an increase in the local Sh_D. Free convection effects on the local Sh_D were found to be insignificant when $Ra_D^+ < 1910$ and $Ra_D^+ < 1750$ for aspect ratios (γ) of 2 and 10, respectively.

Lyczkowski et al. [16] performed a numerical analysis for fully developed laminar forced convection heat transfer in rectangular ducts. The problem was solved for the cases where there was insulation on no walls, one wall, two walls, and three walls with various finite resistances on the remaining walls. The local heat transfer coefficient was determined in the thermal entrance and fully developed regions for constant flux and constant temperature boundary conditions. For the case of one wall at constant temperature and $\gamma = 10$, the fully developed Nusselt number was within 4% of that in Shah and London [17].

The above literature review suggests that convective mass transfer coefficients have been experimentally measured and correlated for turbulent flow through ducts, but not for laminar flow through ducts. In addition, the dependence of the convective mass transfer coefficient on Ra_D when the temperature of the bottom surface of the duct is below that of the airflow has not been reported. Since little information is available at low air speeds, experiments in this paper are predominantly conducted throughout the laminar flow regime. Laminar flow results are compared to the work of [15], to gain an understanding of the effect of bottom wall temperature on the convective mass transfer coefficient. The heat transfer results of [16] and the analogy between heat and mass transfer are used to further verify the present experimental results. Turbulent flow is also investigated up to a Re_D of 8100, so a direct comparison to the work of [9] can be made. In the experiments, the temperature and the relative humidity of the air are also varied so the effect of Ra_D due to the temperature and vapour density differences between the surface of the water and the air stream on the convective mass transfer coefficient can be quantified.

2. Experimental purpose

The purpose of the experiment is to measure the convective mass transfer coefficient between air flowing in a rectangular duct and a pan of water that forms the bottom surface of the duct. The duct is part of a transient moisture transfer (TMT) facility at the University of Saskatchewan, which is designed to study heat and moisture transfer between air and porous building materials [1,18,19]. The convective mass transfer coefficient is an important parameter since it represents the resistance to mass transfer for a particular geometry and is needed for different airflow rates and air relative humidity conditions. There is no correlation in the literature that exactly applies to this facility since free convection effects are present and the airflow is laminar, hydrodynamically fully developed and has thermal and concentration boundary layers that are developing. In this paper, a correlation is developed specifically for the TMT, but it also will allow other researchers to more accurately quantify the mass transfer coefficients for their test facilities that have similar airflow conditions and duct geometry.

3. Experimental apparatus

The transient moisture transfer (TMT) facility is an experimental apparatus that determines the transient heat and moisture transport properties of porous materials. The test section within the TMT is a horizontal rectangular duct, where heat and mass transfer occurs at the bottom wall surface. The facility passes air at varying velocities, temperatures and relative humidities above the surface of materials and measures the change in mass, relative humidity, and temperature in the material as a function of time. To fully document experimental results for the TMT, the convective mass transfer coefficient of this facility is required.

Mass transfer coefficients are usually determined from experiments based on the adiabatic evaporation of a liquid [20] and this method is applied in this paper. Since water vapour transfer is the only form of mass transfer in the TMT facility when experimenting on porous materials, distilled water is used as the evaporating liquid to ensure that the same Schmidt number is present in both experiments. The convective mass transfer coefficient is determined for the horizontal rectangular duct by measuring: (1) the evaporation rate from a rectangular tray of water that is located in the lower panel of the duct and (2) the vapour density difference between the air stream and the surface of the water. The vapour density of the air stream is determined from the measured temperature and relative humidity of the air stream and the vapour density at the surface of the water is determined from the measured temperature of the water and the assumption that the air is saturated at the surface of the water.

A side-view and an expanded top-view schematic of the ducting upstream and downstream of the rectangular test section are shown in Fig. 1(a) and (b). All of the rectangular ducting shown have a width (*W*) of 298 mm. A variable speed vacuum pump supplies a hydrodynamically developed airflow at the entrance of the test section by means of a developing section upstream of the test section (Fig. 1(a)). First, the airflows through a 1100 mm long duct that has a constant cross sectional area, which has several screens installed inside of it to aid in the straightening of the airflow. The air then passes through a 995 mm long converging section that has a convergence angle of 5° to minimize the dynamic losses in the duct and aid in the development of the flow. Following the converging section, the air enters a 500 mm long (13.0 D_h) straight duct that delivers the air to the test section. The air then passes through the 765 mm (19.9 D_h) test section (close-up view shown in Fig. 1(c)) and then through a 890 mm (23.2 D_h) downstream section. The ducts immediately upstream

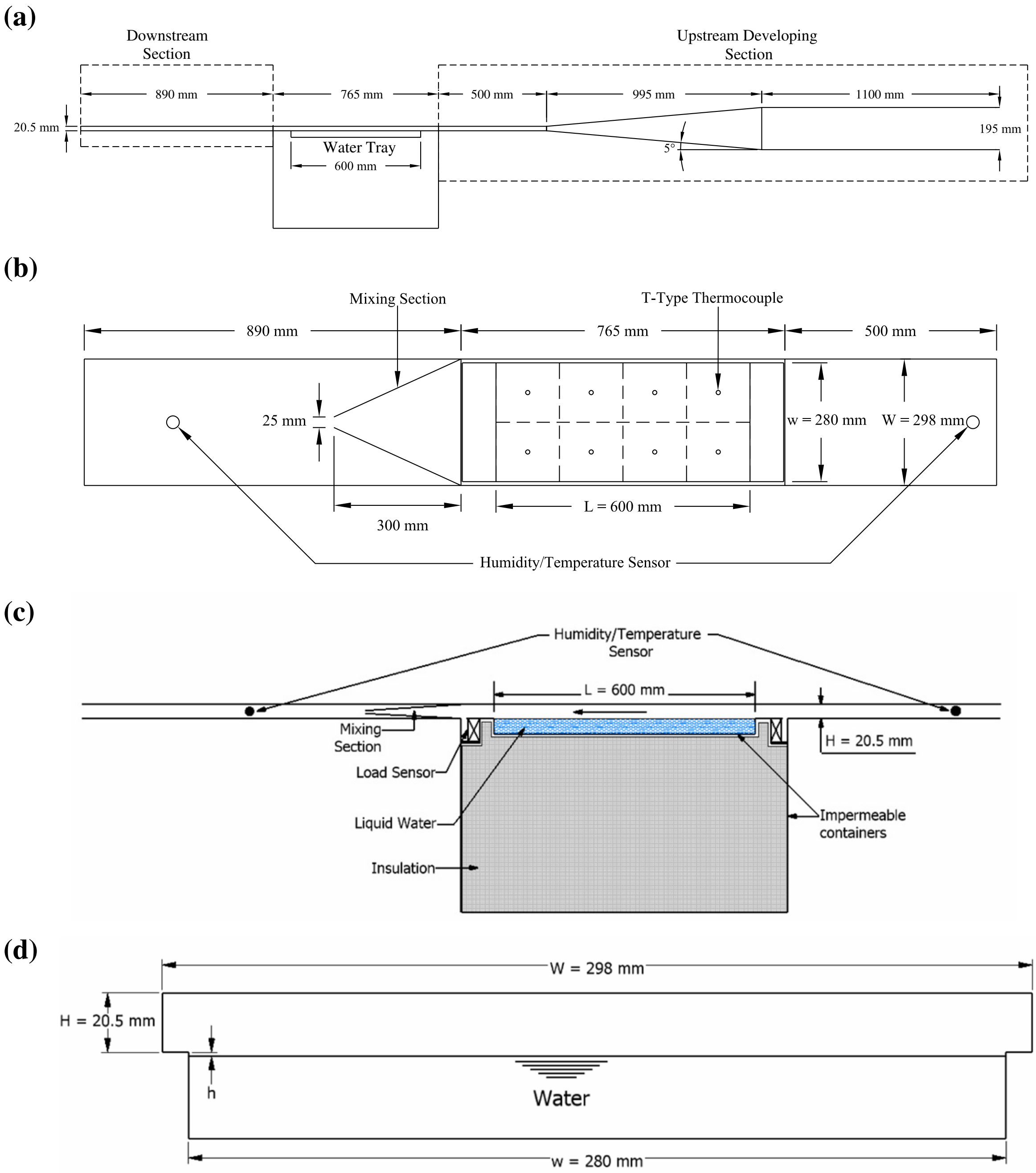

Fig. 1. Schematics of the test facility showing (a) a side view and (b) a top view of the ducting network as well as (c) a side view and (d) a cross-sectional view of the test section.

and downstream of the test section have the same hydraulic diameter as the test section when the evaporation pan is full of water (i.e., $h = 0$ in Fig. 1(d)).

The straightening screens, the small convergence angle (5°) and the 13.0 D_h duct immediately upstream of the test section ensure that the flow is hydrodynamically fully developed for turbulent flow in the duct [21], but the hydrodynamic conditions must be determined experimentally for laminar flow. To determine if the airflow is hydrodynamically developed before it enters the test section, the velocity profile along the height of the duct and the static pressure along the length of the duct immediately upstream of the test section are measured (Fig. 2). Both methods require pressure measurements, which are measured with a pressure transducer. The transducer has a full-scale reading of 0.20 in H_20 (50 Pa), which corresponds to a 5 V output. A pitot-static tube with a tube diameter of 3.06 mm determines the velocity profile within the duct.

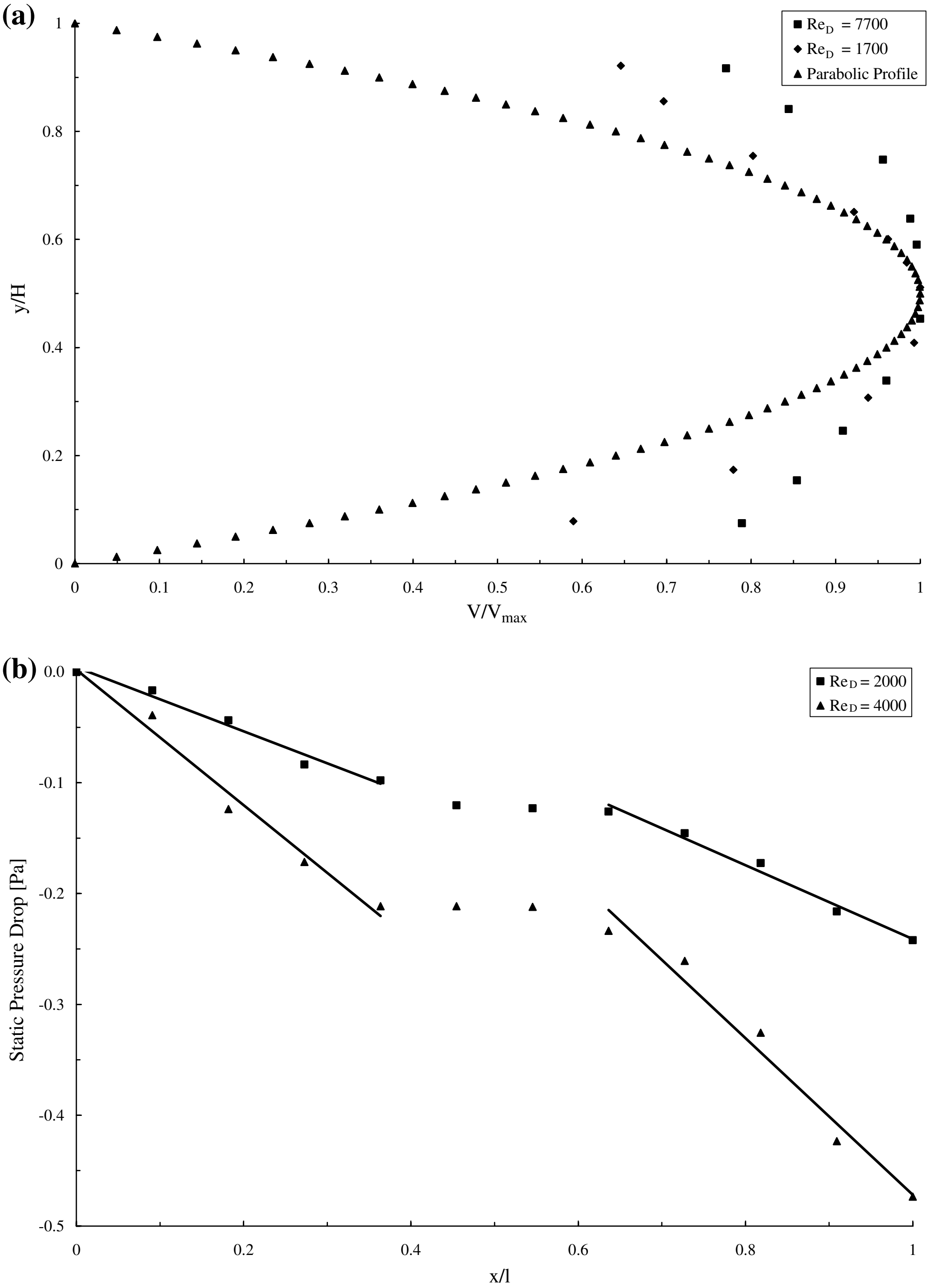

Fig. 2. Measurements of (a) the velocity profile at $x/l = 0.82$ and (b) the static pressure drop along the length of the duct just upstream of the test section, where $x/l = 1$ corresponds to the point where the upstream duct joins the test section.

Transverse velocity measurements over the duct cross-section for laminar ($Re_u = 1700$) and turbulent ($Re_u = 7700$) flow at $x/l = 0.82$ are given in Fig. 2(a). The measurements are quite uncertain because of the small dynamic pressures (0.2–0.6 Pa for laminar flow and 4.2–7.1 Pa for turbulent flow) and the difficulty in determining the exact location of the pitot tube. Nevertheless, the velocity profile for laminar flow forms a velocity profile that is similar to (but broader than) the ideal parabolic Poiseuille velocity profile that is characteristic of fully developed laminar flow. For turbulent flow, the velocity profile has a broader profile than the laminar case, which is characteristic of turbulent flow.

To measure the static pressure profile upstream of the test section, static pressure taps are installed along the centre width of the duct immediately upstream of the test section at intervals of 4 cm, and the pressure difference between each tap and the tap furthest from the test section ($x/l = 0$) is measured. Fig. 2(b) shows pressure data for a Re_u of 2000 and 4000. The static pressure drop varies nearly linear with distance along the duct. The only exception is for 4 cm on either side of the mid point of the duct where the pressure levels. This levelling in pressure is likely due to a slight expansion of the duct near the mid point. The static regain due to even a 1 mm (5%) expansion over a 12 cm region at the mid point of the duct would overcome the friction pressure drop and result in a constant static pressure. The levelling of pressure from $0.4 \leqslant x/l \leqslant 0.65$ may explain why the velocity profile (measured at $x/l = 0.82$ and presented in Fig. 2(a)) is slightly different than the expected parabolic profile for fully developed laminar flow in a rectangular duct.

After the levelling region, the pressure recovers since the pressure drop is slightly larger than the pressure drop before the levelling region. The pressure does not fully recover, however, which indicates that the duct may be slightly larger near the exit. Despite the levelling of the pressure at the midpoint of the duct, the pressure drop becomes linear with distance before the air enters the test section ($x/l = 1$). Since the velocity profile is nearly parabolic (Fig. 2(a)) and the pressure drop is linear at the entrance of the test section (Fig. 2(b)), it is concluded that the airflow entering the test section is hydrodynamically fully developed.

The side and top views of the test section within the TMT facility are also shown in Fig. 1. A tray with a water surface width (w) of 280 mm and a length (L) of 600 mm forms the lower panel of the duct (height (H) = 20.5 mm) in the test section. The air is delivered to the test section from an environmental chamber that controls the temperature and relative humidity of the air upstream of the test section within ±0.1 °C and ±2% RH respectively. The temperature and relative humidity of the air is measured upstream and downstream of the test section with humidity/temperature transmitters. The transmitters' temperature sensors (RTD) are calibrated using a temperature calibrator and have a bias uncertainty of ±0.1 °C. Calibration of the relative humidity is performed using a humidity generator and a chilled mirror as a transfer standard, which has a post calibration bias uncertainty of ±1.0% RH. Since the air is mixed within the environmental chamber and passes through over 2 m of impermeable and adiabatic ducting before it reaches the upstream sensor, the humidity and temperature profile at the upstream sensor (and entering the test section) can be assumed to be uniform. Therefore, the upstream sensor measures the bulk mean relative humidity and temperature of the air entering the test section. On the other hand, the temperature and humidity profiles downstream of the test section will not be uniform and the air must be mixed to obtain the bulk mean properties. Mixing is especially important when there are significant temperature and humidity differences between the air entering the test section and the air in contact with the surface of the water. Mixing is accomplished with the use of a converging duct that is located within the downstream section. The air is mixed by converging the air from the original duct width of 298 mm and height of 20.5 mm into a width of approximately 25 mm and height of 15 mm.

The temperature of the water is measured with eight T-Type thermocouples that are located approximately 2 mm below the surface of the water. The pan is divided into eight imaginary, equally-sized square sections and each thermocouple is placed into the centre of each section (Fig. 1(b)). The temperature readings of the thermocouples are within ±0.1 °C of one another and are averaged to determine the mean surface water temperature. The temperature of the surface of the water is used to determine the average saturated vapour density above the surface of the water [22]. These thermocouples are also calibrated and have a bias uncertainty of ±0.1 °C.

Gravimetric load sensors are used to measure the mass of water that evaporates from the water during the experiment. Four load sensors located at each corner of the tray give a total load capacity of 8 kg with a bias uncertainty of ±2 g. This uncertainty is determined by in situ calibration with calibration masses.

The test section and the ducting connected to it are insulated to minimize any heat transfer with the ambient environment. The top cover above the water pan, which creates the top surface of the test section, is made from 5.08 cm thick polystyrene foam insulation. It is sealed with aluminum foil tape along its edges to ensure there is no leakage of ambient air into or out of the test section during testing. The top cover is also lined with aluminum foil tape to prevent absorption of water vapour, and to reduce the radiative heat transfer between the top cover and the surface of the water. All the ductwork between the upstream and downstream humidity sensors is lined on the inside with foil tape to prevent the absorption of water vapour. Therefore, any change in humidity and temperature between the upstream and downstream sensors will be due to moisture and heat transfer between the free water surface and the air stream.

Located further downstream of the test section is a rectangular to circular transition section that has a circular duct ($D = 72.5$ mm) connected to it (not shown in schematics). The circular duct contains a tapered orifice plate that is located $32D$ downstream of the transition section, and is used to measure the mass flow rate of air within the duct. 15 mm and 30 mm tapered orifice plates are used for the laminar and turbulent flow regimes respectively. The pressure differential across the orifice plate is measured with an electronic pressure transducer with a full-scale reading of 5 in H_2O (1244 Pa) that has a bias uncertainty of ±0.05 in H_2O (12 Pa). The calculation of the mass flow rate using ISO 5167-1 [23] for orifice plates with D and $D/2$ pressure tappings could not be accurately determined, since the standard was not developed for laminar flow at the orifice plate. Therefore, a separate apparatus is constructed in order to calibrate the 15 mm orifice plate for laminar flow.

The apparatus constructed to calibrate the orifice plate consists of two mass flow controllers with a bias uncertainty of ±0.043 g/s each, and circular ducting with the same diameter as the ducting in the TMT facility. Upstream of the orifice plate, ducting with the same length as in the TMT (2.29 m or $32D$) and a longer length (4.58 m or $63D$) are used to determine if there are any flow development effects since the airflow may not be fully developed at the orifice plate within the TMT. A downstream length of 0.90 m ($12D$) is used, since this is the same length in the TMT. Fig. 3 shows the calibration curve for the 15 mm orifice plate, with the two different lengths of upstream pipe. It was found that the length of the upstream section did not produce any appreciable effects. From calibration, the orifice plate produced a 9% increase in mass flow rate, compared to the ISO standard for turbulent flow [23]. From calibration, the mass flow rate equation determined from the measured pressure drop in the experiment for the 15 mm orifice plate is

$$\dot{m} = 0.00017\Delta p^{0.5} \tag{1}$$

and has a bias uncertainty of ±3%.

To improve the accuracy in the turbulent flow regime, the 30 mm orifice plate is also calibrated. The resulting calibration equation is

$$\dot{m} = 0.00069\Delta p^{0.5} \tag{2}$$

and has a bias uncertainty of ±2%.

When performing the main experiment to measure the convective mass transfer coefficient, a range of test conditions are used, but each experimental trial is carried out with constant upstream air properties: temperature, relative humidity and mass flow rate. The temperature of the air upstream of the test section is typically 23 °C, but three tests are performed with an air temperature of 37 °C. The tests cover a range of air relative humidities from 15% to 80%, and Re_D through the test section from 570 to 8100. Measurements of all temperature, relative humidity and pressure readings are recorded every 5 min and the mass change of water in the pan is recorded every 20 min by a computer controlled data acquisition system. All measurement data are an average of 100 measurements taken over 0.1 s intervals at the measured time.

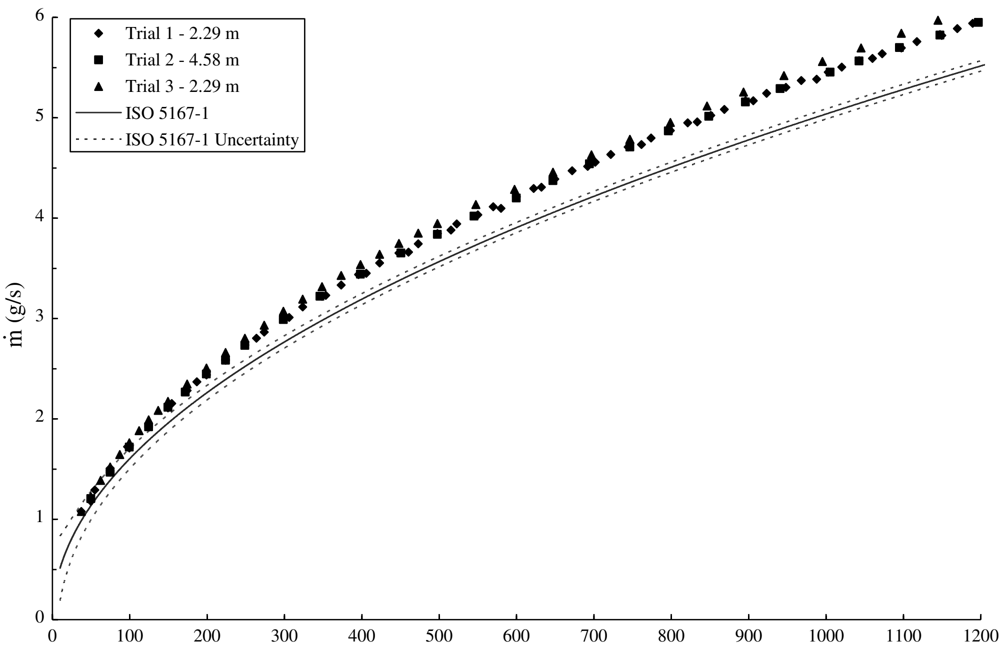

Fig. 3. Calibration data for the 15 mm orifice plate compared to ISO 1567-1 1991 [23] for three trials with different upstream development section lengths. The bias uncertainty in the calibration data is approximately the size of data points on the graph.

4. Data reduction and uncertainty

The main objective of the data reduction is to calculate the independent parameters, Reynolds and Rayleigh numbers and a non-dimensional development length as well as the dependent parameter, Sherwood number (Sh_D), from the experimental data. The 95% confidence intervals for the calculated independent and dependent parameters are determined according to [24], which include both bias and precision uncertainty.

4.1. Reynolds number

The Reynolds number for the experiment is based on the hydraulic diameter of the test section. The cross-section of the test section is shown in Fig. 1(d). The Reynolds number is given as

$$Re_D = \frac{4\dot{m}}{\mu_f P}, \tag{3}$$

where P is the perimeter of the test section duct,

$$P = 2(W + H + h), \tag{4}$$

and $\dot{m}$ is the mass flow rate of air. μ_f is the viscosity of dry air because humidity has a small effect (less than 0.3%) for the conditions in this paper [8,10,25]. μ_f is determined with the Power Law [26] at film temperature (T_f)

$$T_f = \frac{T_s + \frac{T_1+T_2}{2}}{2}. \tag{5}$$

The duct perimeter will vary depending on the average change in height (h) between the top of the pan and the surface of the water during an experimental trial. During most trials, the average change in the water height from the full state is 0.5 mm. This change in height results in a 0.2% increase in the perimeter compared to the full state, which has negligible effect on Re_D during an experimental trial, but is included for completeness. The uncertainty in Re_D for the air flow in the experiment is ±4%, which is mainly due to the uncertainty in the mass flow rate of the air.

4.2. Rayleigh number

Temperature and concentration differences exist between the surface of the water and the bulk airflow. The evaporation process causes the vapour concentration to be highest and the temperature to be lowest at the surface of the water. The resulting density difference between the air–water vapour mixture at the surface of the water and in the bulk air stream results in natural convection, which can be quantified with a Rayleigh number (Ra_D) defined as

$$Ra_D = \left[\frac{g\bar{\rho}_g(\rho_{g,s} - \rho_{g,\infty})D_h^3}{\mu_f^2}\right]Sc, \tag{6}$$

where D_h is the average hydraulic diameter of the test section during the test, which varies depending on the average change in height (h) of water during an experimental trail:

$$D_h = \frac{4(WH + wh)}{2(W + H + h)}. \tag{7}$$

The uncertainty in D_h for this experiment is ±2%. It should be noted that the change in height ($h = 0.5$ mm) accounts for a 2% increase in the hydraulic diameter compared to that of the full state. The density of moist air at the surface of the water ($\rho_{g,s}$) is based on the sum of the partial densities of water vapour and dry air at the surface of the water

$$\rho_{g,s} = \rho_{v,s} + \rho_{a,s}. \tag{8}$$

The partial pressure of water vapour at the surface of the water ($p_{v,s}$) is calculated using psychrometrics [22], where

$$p_{v,s} = p_{sat}(T_s). \tag{9}$$

The partial pressure of air at the surface of the water ($p_{a,s}$) is calculated assuming that the total pressure (p_g) is constant,

$$p_{a,s} = p_g - p_{v,s}. \tag{10}$$

The total pressure is measured in the laboratory with a mercury barometer during each experimental trial. The ideal gas law is used to determine $\rho_{v,s}$ and $\rho_{a,s}$ at T_s. The density of moist air in the ambient ($\rho_{g,\infty}$) is a measure of the average of the inlet and outlet densities,

$$\rho_{g,\infty} = \frac{\rho_{g,1} + \rho_{g,2}}{2}. \tag{11}$$

With the use of the ideal gas law and the measurements of the relative humidity and dry bulb temperatures upstream and downstream of the test section, the water vapour and dry air densities are determined at these two locations. The partial pressure of water vapour is determined by:

$$p_{v,i} = \phi_i p_{sat}(T_i), \tag{12}$$

$$p_{a,i} = p_g - p_{v,i}, \tag{13}$$

where $i = 1$ at the inlet and $i = 2$ at the outlet of the test section. The mean mixture density of air in the boundary layer ($\bar{\rho}_g$) is

$$\bar{\rho}_g = \frac{\rho_{g,s} + \rho_{g,\infty}}{2}. \tag{14}$$

The bias uncertainty in Ra_D is ±8%, which is mainly due to the uncertainty in D_h.

4.3. Inverse Graetz number

A dimensionless axial distance (X^*) in the flow direction for the entrance region is typically specified as the inverse of the Graetz number (Gz). For mass transfer,

$$X^* = \frac{L}{D_h Re_D Sc} = \frac{1}{Gz}. \tag{15}$$

The concentration boundary layer is considered to be developing for $X^* < 0.05$, and in this paper the maximum value of X^* is 0.04. The bias uncertainty in X^* is ±5%.

4.4. Sherwood number

The Sherwood numbers (Sh_D) are based on the hydraulic diameter of the test section (Eq. (7)) and are determined from the measured data.

$$Sh_D = \frac{h_m D_h}{D_{AB}}, \tag{16}$$

where the convective mass transfer coefficient (h_m) depends on the measured evaporation rate of water ($\dot{m}_{\text{evap}}$), the surface area of the pan ($A_s = wL$), and the log mean vapour density difference ($\Delta\rho_v$) between the bulk air and the surface of the water.

$$h_m = \frac{\dot{m}_{\text{evap}}}{A_s \Delta\rho_v} \tag{17}$$

$$\Delta\rho_v = \frac{(\rho_{v,s} - \rho_{v,2}) - (\rho_{v,s} - \rho_{v,1})}{\ln[(\rho_{v,s} - \rho_{v,2})/(\rho_{v,s} - \rho_{v,1})]}. \tag{18}$$

The binary diffusion coefficient (D_{AB}) for water vapour in air depends on T_f and p_g and is calculated from [22]. The 95% confidence intervals for Sh_D are strongly dependent on the log mean density difference between the air and the water ($\Delta\rho_v$), and the evaporation rate ($\dot{m}_{\text{evap}}$). For the range of test conditions in this paper, $\dot{m}_{\text{evap}}$ and $\Delta\rho_v$ have bias uncertainties in the range of ±1% to ±5% and ±2% to ±8%, respectively, resulting in bias uncertainties in Sh_D of ±3% to ±9%.

4.5. Mass and energy balances across the test section

In any experiment, it is important to verify that mass and energy are conserved. Applying the basic principles of conservation of mass and energy over a control volume can help determine how well the experiment is setup to measure heat and mass transfer, and identify bias errors in the experiment. It is important that mass and energy balances are satisfied within experimental uncertainties. If the mass and energy balances are not satisfied within the experimental uncertainties, systematic errors exists within the experiment, such as heat and mass transfer with the ambient environment or improper setup of the experiment and instruments, or the measurement uncertainties have been underestimated.

As noted previously, it is essential to mix the air leaving the test section to accurately measure the bulk relative humidity and temperature. In the experiment, the evaporation of water from the tray is measured using load sensors and the change in humidity of the air stream is measured with humidity sensors. By comparing the evaporation measured with the load sensors to the moisture gained by the air as it travels through the test section, as measured by the humidity sensors, the adequacy of the mixing section downstream of the test section (Fig. 1(b)) can be determined. The mass balance is satisfied within the experimental uncertainties for all tests when the mixing section is used and when the humidity of the air entering the test section (ϕ_1) exceeds 80% RH regardless of whether the mixing section is used or not. When $\phi_1 > 80\%$ RH, the water vapour density difference between the surface of the water and the airstream entering the test section is small and the downstream mixing section has a small effect on the results because the vapour density is quite uniform in the boundary layer. On the other hand, the mass balance is not satisfied within the experimental uncertainty when the mixing section is not used and $\phi_1 < 80\%$ RH. The bias uncertainty in the evaporation rate determined using load sensors (±1%–±5%) is as much as 10 times lower than the bias uncertainty in the evaporation rate determined using the measured humidity and temperature difference between the inlet and outlet air streams. Therefore, the outlet conditions can be accurately calculated by applying mass and energy balances across the test section using the evaporation rate measured by the load sensors. If the outlet temperature and relative humidity conditions of the airstream are calculated in this way, Sh_D changes by less than ±4% compared to the case where Sh_D is determined using the outlet conditions measured downstream of the mixing section. This is within the experimental uncertainty and verifies the energy and mass balances in the experiment. A similar good agreement exists for the tests when $\phi_1 > 80\%$ RH with or without the mixing section. In the tests where the mixing section is not used, Sh_D is as much as ±16% different when using the calculated and measured outlet air temperature and humidities. As this is outside the 95% confidence limits for this experiment, it indicates a systematic error when the mixing section is not used.

About half of the tests were performed without the mixing section and with $\phi_1 < 80\%$ RH, resulting in mass balances outside the experimental uncertainty. Instead of rejecting these data, a Sh_D based on the calculated outlet air conditions are used for these experiments. The bias uncertainty associated with this calculation increases the uncertainty in Sh_D by 1%–6% (depending on the vapour density difference between the air and the water surface) and is included in the reported uncertainty values.

A measure of the importance of the energy transport through mass diffusion relative to that through thermal diffusion is represented by S^* [14,15], where

$$S^* = \frac{\rho_g D_{AB} h_{fg} \Delta W}{k_g \Delta T}. \tag{19}$$

S^* is a result of simultaneous heat and mass transfer due to the evaporation process, which varies throughout the experiment depending on the conditions of the air entering the test section. This dimensionless parameter is similar to the dimensionless operating condition factor [27,28]

$$H^* = 2500 \frac{\Delta W}{\Delta T}, \tag{20}$$

where

$$\Delta W = W_s - W_1 \tag{21}$$

$$\Delta T = T_s - T_1, \tag{22}$$

and the coefficient (2500) has units of kg K/kg. H^* accounts for the coupling between heat and moisture transfer and varies between −3.6 and −1.4 for the experimental conditions in this paper. The differences between H^* calculated with Eq. (20) and S^* calculated with Eq. (19) are less than ±0.3, and the small differences are mainly due to the constant properties used in calculating the coefficient of 2500 kg K/kg in Eq. (20). Since H^* is an important parameter when correlating the effectiveness of air-to-air energy exchangers [27,29], it will be used in this paper as well to correlate Sh_D and show the effect of operating conditions on the convective mass transfer coefficient.

5. Results and discussion

The following section will present experimental data from a laminar and turbulent test, showing the pre-test transient period and the steady state period. These data will show when steady state has been achieved, and will help quantify the precision uncertainty of the experiment. Following this, a summary of the Sh_D data obtained during the steady state period for a range of test conditions as well as the correlations developed from these data are provided. A comparison to data in the literature is also provided.

5.1. Transient data and precision uncertainty

A steady state energy balance results when the evaporation of water reduces the temperature of the water to a point where the heat transfer from the air to the water equals the heat required to evaporate water from the pan. Prior to this, the experiment is in a transient state as shown in Figs. 4–6 for tests performed at a Re_D of 1500 and 6000. Fig. 4 shows the temperature measurements of air at the inlet and outlet of the test section as well as the average temperature of the water surface. Fig. 4 shows that at the beginning of the test, the water in the tray has an initial temperature of approximately 20 °C, and once the airflow passes through the test section, evaporation reduces the temperature of the water and the air leaving the test section. The water and air temperatures continue to decrease until an equilibrium (or steady) state exists, where the heat loss from the air equals the heat required to evaporate the water. Steady state is determined by selecting (based on visual inspection) a period during the experiment when all measurements are steady with time. In Fig. 4, the time selected to reach steady state is greater for laminar flow (15 h) than for turbulent flow (11 h). All individual air temperature data points are within ±0.1 °C from the mean and the water temperature data points are ±0.1°C from the mean between 15 h and 21 h for laminar flow and 11 h and 16 h for turbulent flow. In Fig. 5, the relative humidity measurements are within ±0.2% RH during the same time periods. Since the fluctuations of the measurements shown in Figs. 4 and 5 are small during these time periods, steady state is deemed to occur.

The mass of water that evaporates during the experimental period is shown in Fig. 6(a). The water height is level with the top of the pan at a mass of approximately 7200 g, which is found by measuring the height (30 mm) of the water in the centre of the pan. During the experiment, water evaporates from the pan and is periodically filled during the transient period to keep the pan as full as possible during the steady state portion. The instantaneous changes in mass in Fig. 6(a) at $t \approx 3$ h and $t \approx 8$ h are a result of the pan being filled to make up for any evaporated water during the test. The pan is slightly over filled (i.e., above 7200 g) to decrease the number of times the pan has to be filled before the steady state period begins. A linear curve fit is performed on the data during the steady state periods to determine the average evaporation rate during this time. The linear curve fits give a correlation coefficient (r^2) of 0.997 for $Re_D = 1500$ and 1.000 for $Re_D = 6000$, suggesting that the evaporation rate is constant during the steady state periods. The 95% precision uncertainty in the average value of $\dot{m}_{\text{evap}}$ is ±0.4 g/h (±2.4%) for $Re_D = 1500$ and ±0.5 g/h (±1.1%) for $Re_D = 6000$ during the steady state period. Fig. 6(b) shows the average mass evaporation rate over 2 h time periods for the two experimental trials. For example, for 1 h, data are averaged over hours 0 and 2. At first, the evaporation rates are the greatest since the water temperatures are the highest at the beginning of the trial, but then decrease as the water temperatures reduce. During the steady state period, the 95% precision uncertainty (tSEE) in Fig. 6(b) is ±3 g/h (±17%) for $Re_D = 1500$ and ±1.7 g/h (±4%) for $Re_D = 6000$.

Fig. 6(c) presents Sh_D as a function of time during the experiments by averaging the temperature, relative humidity and mass measurements over 2 h periods. Here $\dot{m}_{\text{evap}}$ is determined from Fig. 6(b) and therefore the profiles of $\dot{m}_{\text{evap}}$ and Sh_D are relatively similar, especially after the experiment has started to run for a few hours. If $\dot{m}_{\text{evap}}$ is determined using the slope in Fig. 6(a), the results change little and are not presented. During the steady state period, the average Sh_D calculated from the 2 h averages in Fig. 6(c) (i.e., based on Fig. 6(b)) is within ±1.5% ($Re_D = 1500$) and ±0.2% ($Re_D = 6000$) of the average Sh_D that is determined using the slope in Fig. 6(a). Since the hourly Sh_D does not vary greatly over the steady state time period, the experimental data are averaged over the entire steady state time period, and one Sh_D is calculated for each test condition. The evaporation rate is determined using the slope (e.g., Fig. 6(a)) because it results in the smallest precision uncertainty (±3%) in Sh_D.

The repeatability of the experiment is determined from two different sets of data, one for turbulent flow, and one for laminar, by comparing experimental trials with similar test conditions. At a $Re_D = 1410$ and 4300, Sh_D was repeatable within ±1.1% and ±2.4% respectively, when the relative

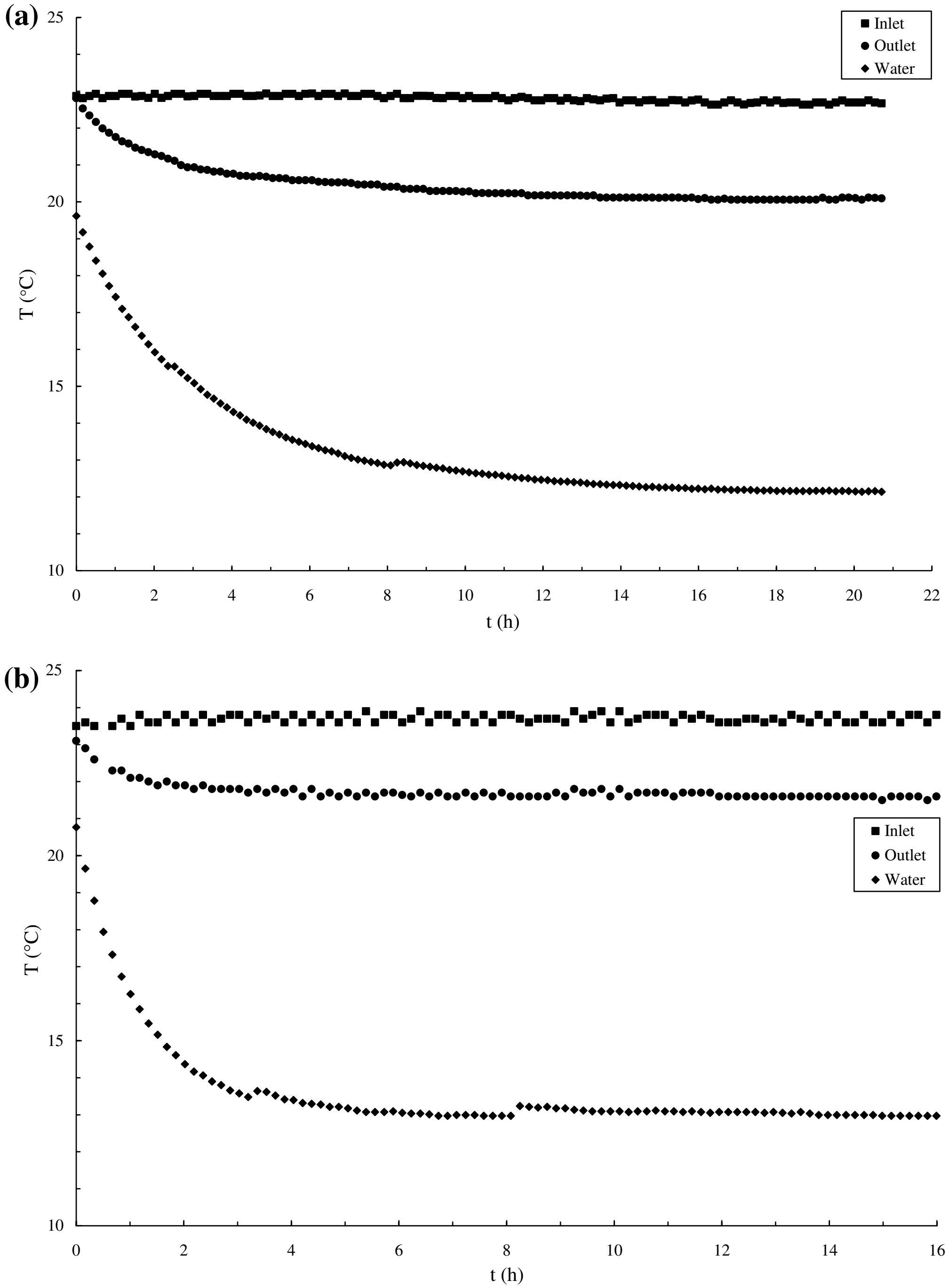

Fig. 4. Temperature of the air entering and leaving the test section and the average surface temperature of the water for (a) $Re_D = 1500$ and (b) $Re_D = 6000$.

humidity and temperature difference of the airflow entering the test section between two trials are less than 3% RH and 0.1 °C. Sh_D compares well when similar operating conditions exist, which shows the high repeatability of the experiment and confirms the precision uncertainty of ±3% in Sh_D.

Steady state operating conditions are important since they allow an averaged convective mass transfer coefficient to be determined over the testing time period for a specific set of relative humidity, temperature and mass flowrate conditions of the upstream airflow. The test procedure allows steady state conditions to be achieved by operating the experiment until the temperature and relative humidity of the air and the water temperature are viewed to be constant. The water that evaporates from the pan during this time period is replaced until steady state conditions are observed. After steady state conditions are reached, each test is conducted for four to eight hours and the data acquired are averaged over this time span.

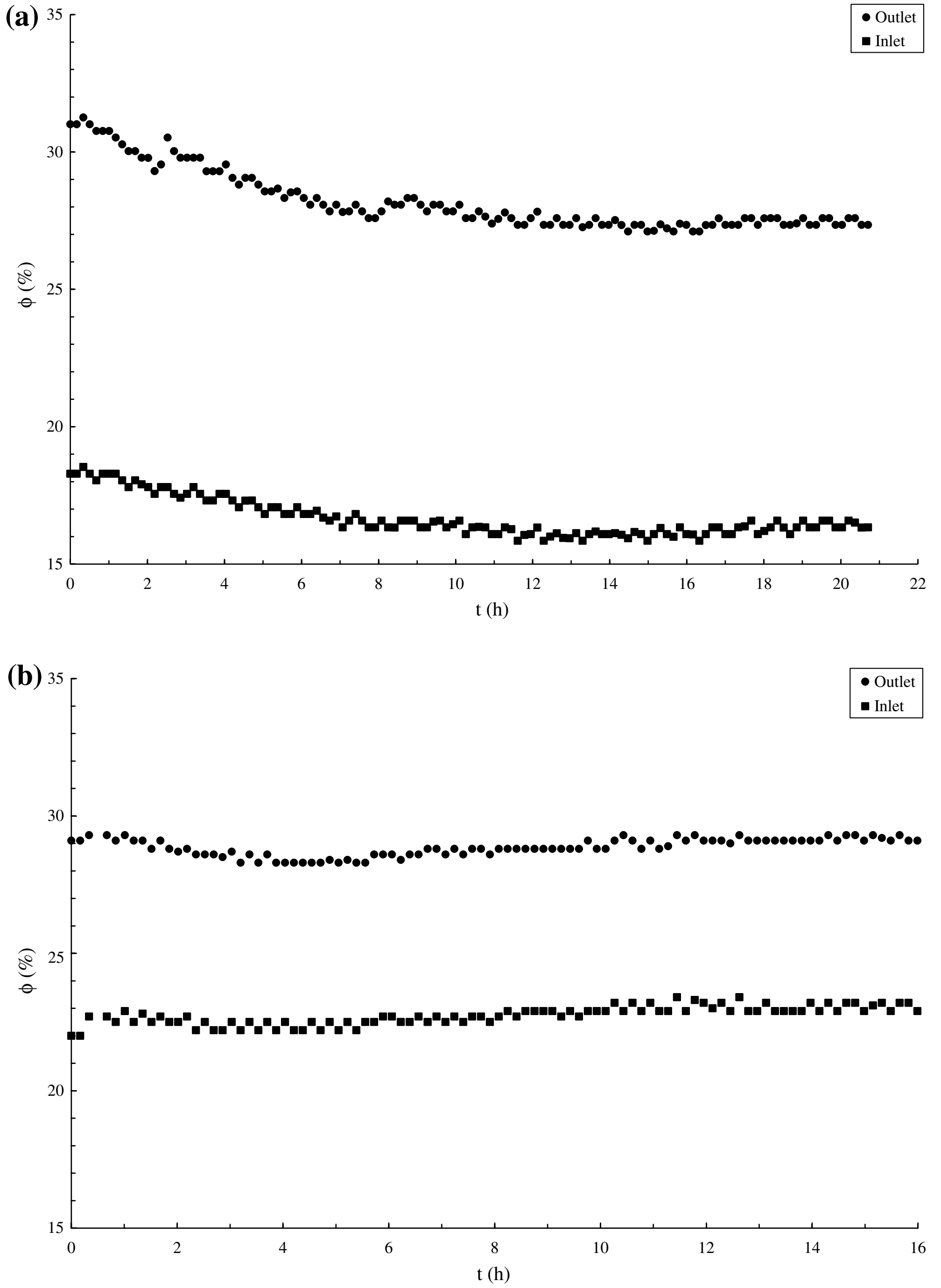

Fig. 5. Relative humidity of the air entering and leaving the test section for (a) $Re_D = 1500$ and (b) $Re_D = 6000$.

5.2. Steady state data

5.2.1. Laminar flow

The Sh_D is determined for laminar flow between a Re_D of 570 and 2100, which corresponds to a X^* between 0.011 and 0.037, and a Ra_D of 6300 and 83,000 ($0.003 < Gr_m/Re_D^2 < 0.2$), and is presented in Fig. 7. Fig. 7(a) shows a general trend of increasing Sh_D as Re_D increases (X^* decreases), which is expected [30] since the test section is not long enough for the temperature and concentration boundary layers to become fully developed. As Re_D increases, the thermal and concentration boundary layers become thinner and less developed over the surface of the water. A thinner boundary layer results in a larger concentration gradient at the surface of the water, which contributes to an increase in forced convection mass transfer at the surface of the water.

Fig. 7(a) also shows that there is a large variation in Sh_D and the uncertainty in Sh_D for a given X^*. The values of Sh_D range from 4 to 8 and the total uncertainties in Sh_D

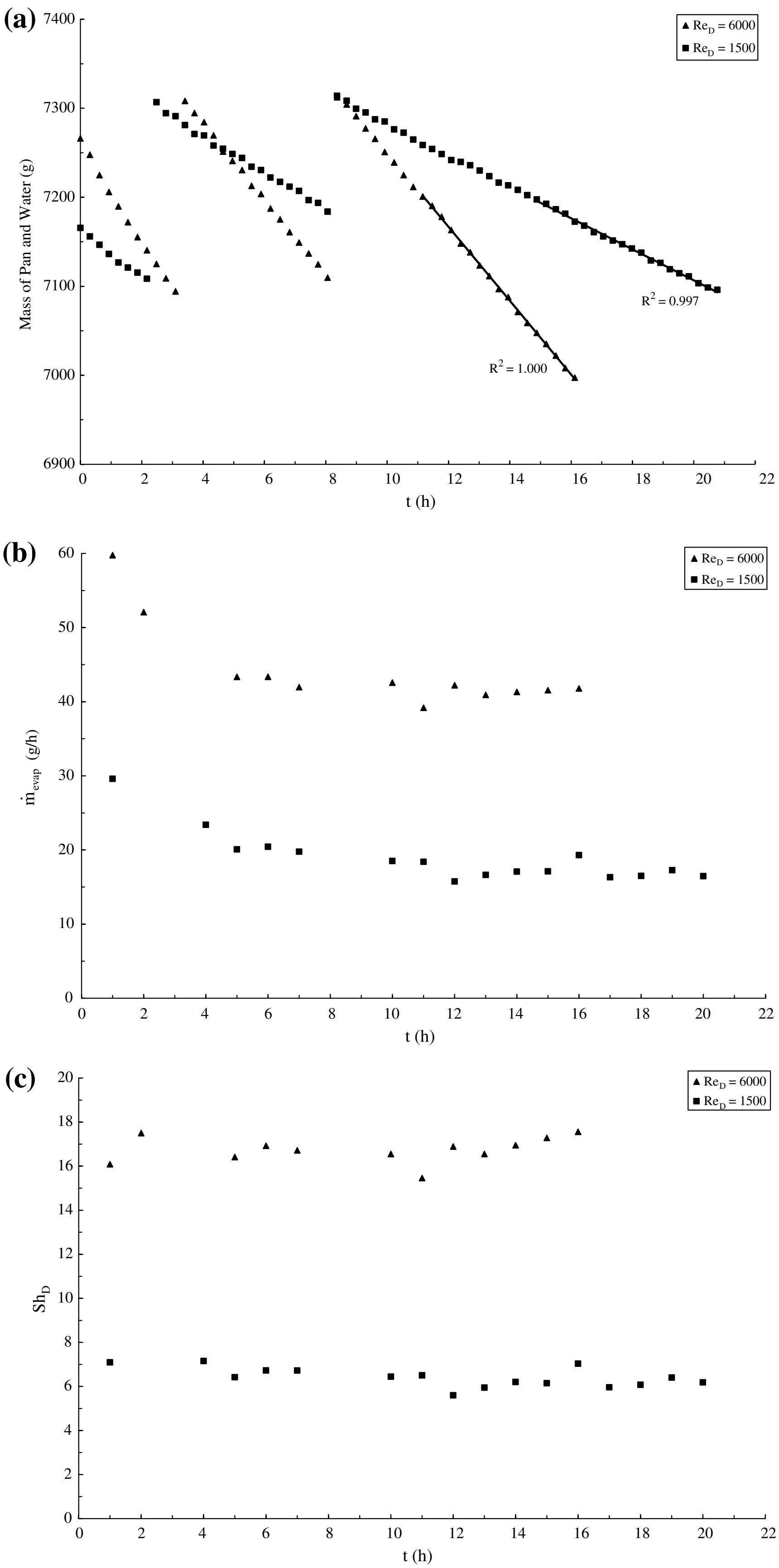

Fig. 6. Measured (a) weight of the water tray and (b) evaporation rate of water and (c) calculated Sherwood number for tests with laminar and turbulent flow. The discontinuities are a result of the water tray being filled during the transient period of the experiment.

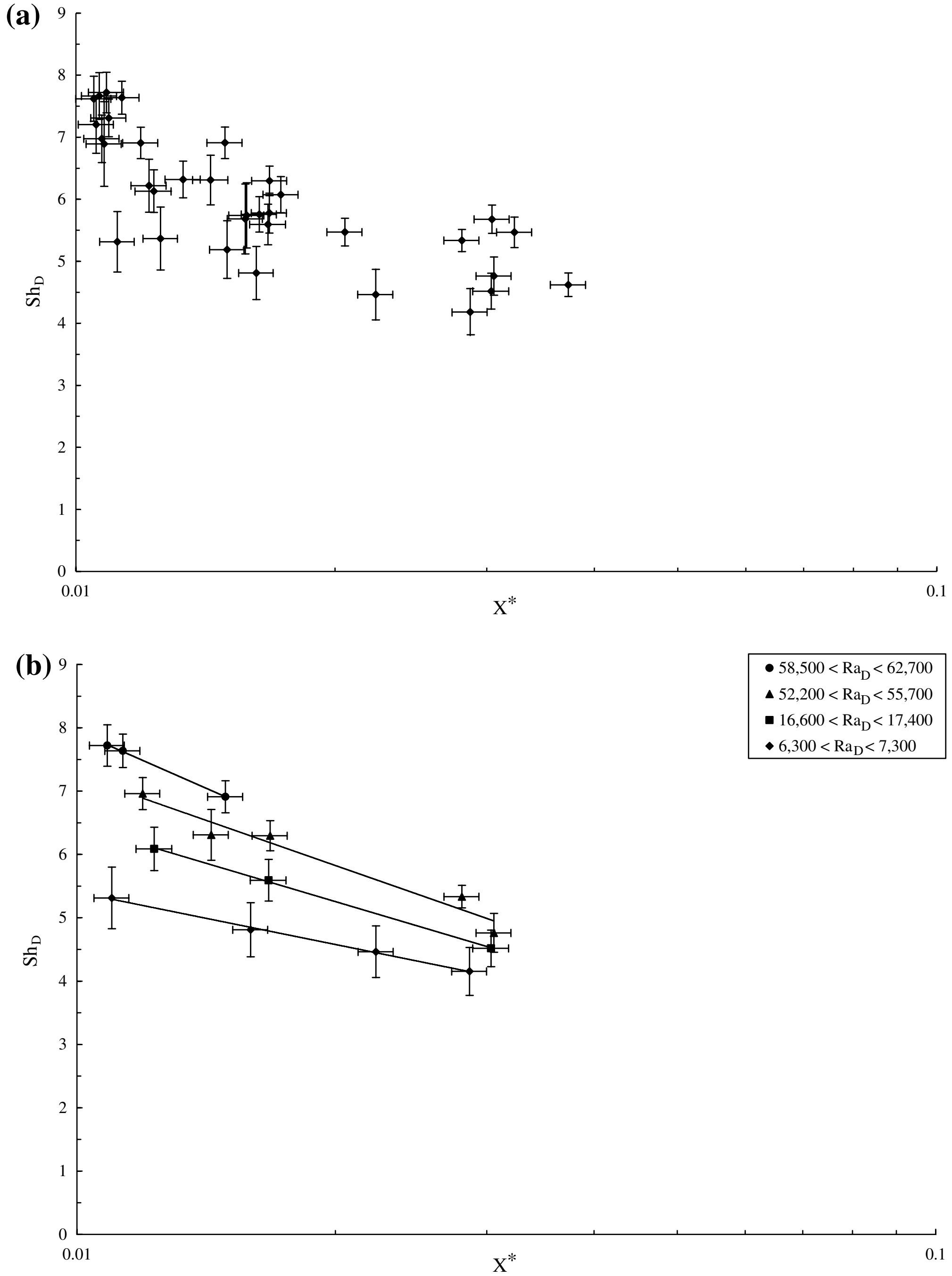

Fig. 7. Laminar flow results of Sherwood number for a range X^* and Rayleigh numbers (Ra_D) for (a) all the experimental tests and (b) specific ranges of Ra_D, where the variation in Ra_D is less than ±10% in each group.

range from ±3% to ±13% with only 6 (out of 35) values exceeding ±10%. This scatter is a result of each data point having a unique Ra_D associated with it. Since the temperature of the water is not controlled during the experiments, but is dependent on the phase change rate, Ra_D cannot be precisely controlled from one experimental trial to the other. To determine if Sh_D is dependent on Ra_D, Fig. 7(b) shows four curve fits to data over a small range of Ra_D. The data for a range of Ra_D are within ±10% of the average Ra_D for that range.

The data in Fig. 7(b) show that as Ra_D increases, Sh_D increases and the uncertainty in Sh_D decreases. In this experiment, the density of the moist air at the surface of the water is always larger than that of the bulk airflow, since the water temperature is always less than the bulk airflow temperature, which causes a buoyancy-driven downflow of air towards the surface of the water [12]. Sparrow et al. [12] found that this type of downward airflow dominated the evaporation of water from circular pans when the water temperature was less than the ambient air temperature. Other researchers have demonstrated the importance of natural convection heat transfer for thermal developing flow in rectangular ducts. Refs. [31,32] show the secondary flow patterns that result as cooled air flows down the wall and recirculates in the centre of the duct or cavity. A similar flow pattern is expected in this experiment, which may be enhanced by non-uniform conditions in the experiment [32].

In this study, as the relative humidity of the air delivered to the test section decreases for a constant X^*, the temperature at the surface of the water decreases. For the experiments in this paper, the water temperature is 1–14 °C colder than the bulk air temperature, depending on the relative humidity, temperature and Re_D of the airflow. A decrease in the relative humidity of the bulk airflow results in an increase in the vapour concentration difference between the bulk airflow and the surface of the water. Also, a decrease in water temperature causes the moist air (air–water vapour mixture) density difference between the bulk airflow and that at the surface of the water to increase, which results in an increase in Ra_D (Eq. (6)). The effect of the air relative humidity and the temperature of water suggests that evaporation is greater with dry air than with humid air [13,14], due to the simultaneous increase in the vapour concentration difference and Ra_D. The combined effects of natural convection and the effectiveness of the relative humidity of the airflow on the evaporation process influences the convective mass transfer coefficient and these effects are represented well by Ra_D.

From the experimental data, it is found that Sh_D has a dependence on X^* and Ra_D. A curve fit to the data shown in Fig. 7(a) results in

$$Sh_D = 0.417\frac{Ra_D^{0.124}}{X^{*0.334}}, \tag{23}$$

where $r^2 = 0.90$ and 95% of the experimental data fall within ±10.0% of the correlated line.

As noted previously, the temperature and humidity of the air entering the test section influences Ra_D as well as S^* (Eq. (19)) and H^* (Eq. (20)). Therefore, the temperature and humidity of the airflow cannot be neglected for simultaneous heat and moisture transfer. In fact, it is equally possible to correlate Sh_D with H^* (or S^*). The correlation that results is

$$Sh_D = \frac{2.11}{X^{*0.308}|H^*|^{0.371}}, \tag{24}$$

which is valid over the experimental testing range of $-3.6 < H^* < -1.4$, which corresponds to reduced mass transfer because the thermal and moisture transfer (or buoyancy forces) are in opposite directions [33]. Eq. (24) fits the experimental data with an r^2 of 0.89 and 95% of the experimental data fall within ±9.4%.

In order to increase confidence in the experimental data (Fig. 7) and correlation Eqs. (23) and (24), they are compared with data in the literature in Fig. 8. Fig. 8(a) shows a reasonable agreement between the numerical results of Lin et al. [15] and the present work. However, Sh_D calculated by Lin et al. [15] is slightly larger than Sh_D measured in this paper for the same value of Ra_D. The reason for the higher Sh_D in [15] is that the numerical results were determined for evaporation from heated water rather than cooled water as in the current experiment. Heated water creates an upward natural convection airflow, which results in a greater convective transfer coefficient than in the present study which has a cooled water surface. This is well known for free convection heat transfer from the top surface of hot and cold horizontal plates [30] and therefore Fig. 8(a) helps confirm the validity of the correlation developed in this paper (Eq. (23)).

Another useful comparison is to compare the measured mass transfer coefficients with heat transfer coefficients from the literature using the analogy between heat and mass transfer with

$$Sh_D = Nu_D\left(\frac{Sc}{Pr}\right)^{1/3}. \tag{25}$$

Eq. (25) is valid when mass transfer rates are low. When mass transfer rates and the bulk fluid motion required to overcome the diffusion of air to the water surface are high, Eq. (25) needs to be corrected [34]. For the range of testing conditions in this paper, the maximum correction of Eq. (25) is 1% [34]. Since the correction is small, the experiments are considered to be low mass transfer experiments and Eq. (25) is used without any correction.

The study in the literature that most closely represents the current experiment is a numerical study of laminar flow forced convection heat transfer within a heated rectangular duct [16]. The flow is hydrodynamically developed and thermally developing, but natural convection is neglected. To compare the results for one heated wall based on the 1/2 height of the duct, the Nusselt number in [16] must be converted to a Nusselt number based on the hydraulic diameter by multiplying the former by $4/(1 + 1/\gamma)$.

A comparison between the predicted mass transfer results of [16] and the present study are given in Fig. 8(b). It is shown that the results of [16] are within the range of measured Sherwood numbers, and compare well at the upper range of Rayleigh numbers. This comparison shows that the work of [16] predicts Sh_D within the range of experiment results, but the effects of buoyancy (Ra_D) and the relative strengths of heat and mass transfer due to the operating conditions (H^*) are not accounted for. By neglecting the effects of Ra_D or H^*, the error in Sh_D can be up to 30%. This difference may be due to the fact that the analogy between heat and mass transfer cannot account for the operating conditions (H^*) or systematic errors such as heat transfer between the test section and the environment or unsaturated air at the surface of the water.

5.2.2. Turbulent flow

Turbulent flow experiments are performed in order to develop a relationship for Sh_D that includes both developing

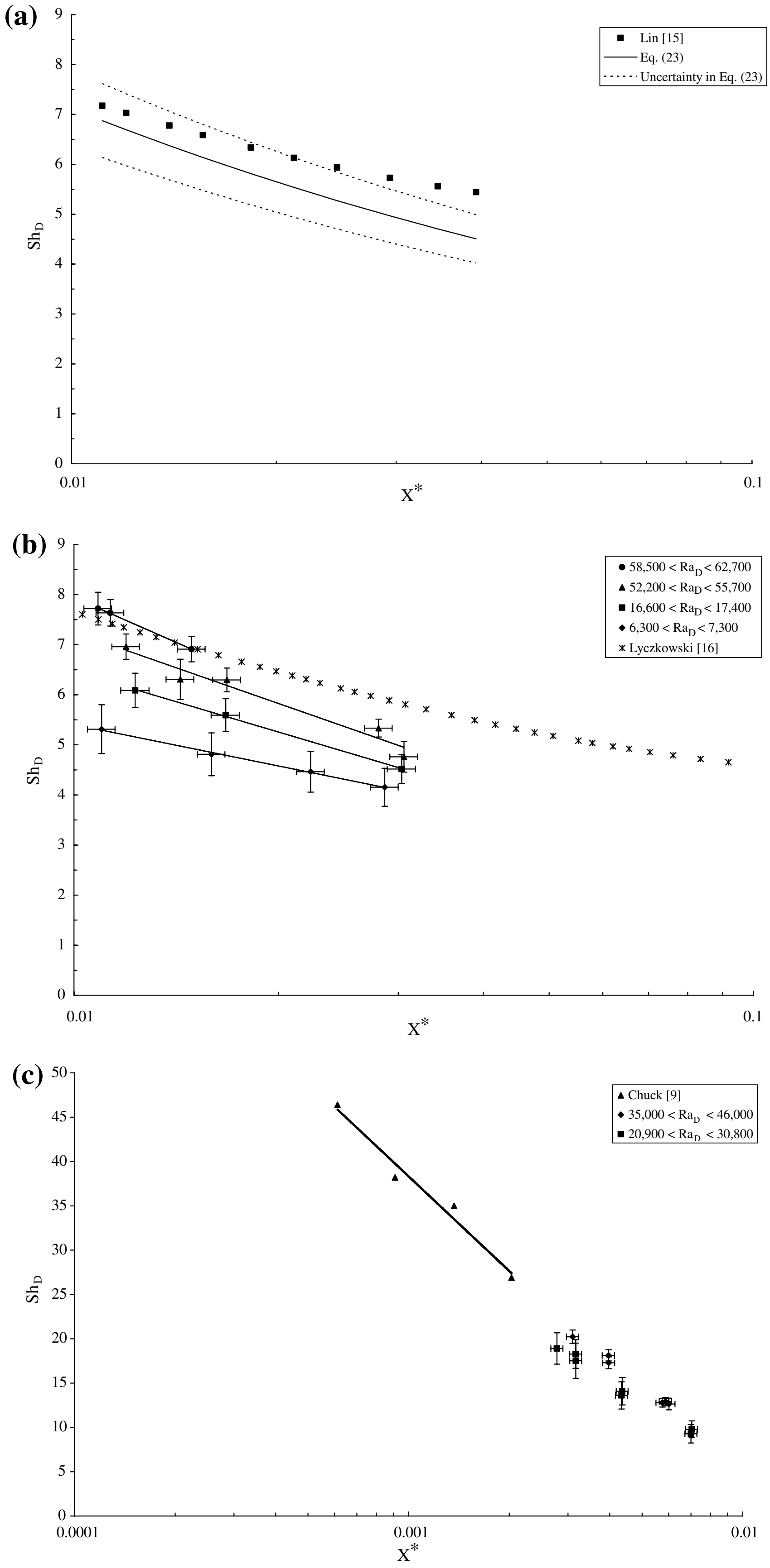

Fig. 8. Comparison of the Sh_D determined in this paper with (a) Lin et al. [14] when $Ra_D = 35,300$, (b) Lyczkowski et al. [15] and (c) Chuck [8].

flow (X^*) and buoyancy forces (Ra_D), and also to further verify the experiments by comparing to experiments in the literature [8,9], which are for turbulent flow. The turbulent flow data of the present work cover a range of Re_D between 3100 and 8100, and Ra_D between 20,900 and 46,000. The various Ra_D are created by the air relative humidity between 15% RH and 60% RH at a constant air temperature of 23 °C. The results in Fig. 8(c) show that as Ra_D increases, Sh_D increases. The contribution of natural convection compared to that of forced convection is measured by Gr_{m}/Re_D^2. This ratio is approximately 20 times less than that for the laminar flow experiments, which suggests that the contribution of natural convection evaporation is smaller in the presence of forced convection turbulent flow than in laminar flow. Nevertheless, the effects of Ra_D exists and the experimental data in the turbulent region are correlated with X^* and Ra_D, which results in

$$Sh_D = 0.012\frac{Ra_D^{0.311}}{X^{*0.725}}, \tag{26}$$

where $r^2 = 0.98$, and 95% of the data are within ±7.1% of the correlated line.

If H^* is correlated with the experimental results,

$$Sh_D = \frac{0.382}{X^{*0.719}|H^*|^{0.494}}, \tag{27}$$

which is valid over a range of $-2.1 < H^* < -1.4$. Eq. (27) fits the experimental data with an r^2 of 0.99, and 95% of the experimental data are within ±3.5%. The curve fit of Eq. (27) has better agreement than Eq. (26), which suggests that for turbulent flow, the operating condition factor (H^*) may be a better fitting parameter than Ra_D.

Experimental data of [9] are shown in Fig. 8(c) for test section lengths of 12.5 cm and 27.9 cm at a Re_D of 7200 and 10,700. Since the data of [9] are for step heights (h) ranging from 3.8 mm to 15.2 mm, the experimental results of [9] are extrapolated to $h = 0$ mm for comparison to the present work. Even though the average h in the present work is 0.5 mm, there is no seen effect on Sh_D when neglecting this small height drop in the pan of water. A linear decreasing Sh_D with increasing X^* for both studies confirms that the concentration boundary layers within the ducts are not fully developed. A linear curve fit of the data in [9] fits well with the present work, especially for the larger range of Ra_D (35,000–46,000). The testing conditions for the larger range of Ra_D occurs when $15\% < \phi_1 < 30\%$, and the testing conditions of [9] are within this range.

6. Conclusions

Combined forced and natural convection evaporation from a filled pan situated in the lower panel of a rectangular duct is investigated experimentally. Mass transfer measurements are made for a hydrodynamically developed airflow with developing concentration and thermal boundary layers. The effects of forced convection evaporation is investigated by varying the velocity of the air passing through the duct in the laminar and turbulent flow regimes between a Re_D of 570 and 8100. The effect of the density difference between the bulk flow and the air at the surface of the water is determined for Re_D between 6300 and 83,000. The convective mass transfer coefficient is dependent on the strength of natural convection, as well the temperature and humidity of the bulk airflow. The effect of the temperature and humidity of the air stream can be accounted for using the operating condition factor H^* or S^*, which are a ratio of the heat and moisture transfer potentials in the experiment. A correlation for Sh_D as a function of X^* and Ra_D is developed to account for the effects of forced and natural convection as well as entrance region effects on the evaporation process for laminar and turbulent airflow. The correlation in the laminar flow region is $Sh_D = 0.417Ra_D^{0.124}/X^{*0.334}$ with a 95% confidence limit of ±10.0%, and the correlation in the turbulent flow regime is $Sh_D = 0.012Ra_D^{0.311}/X^{*0.725}$, with a 95% confidence limit of ±7.1%.

The experimental data in this paper compare favourably to numerical and experimental data in the literature. These comparisons show that the magnitude and direction of heat and mass transfer affect Sh_D. Sh_D is always larger when the surface of the duct is heated above that of the air, than when it is cooled below the temperature of the air. Therefore, this paper extends the literature for the case of a cooled water surface. The comparisons also show that it is possible to use Nu_D data from the literature together with the analogy between heat and mass transfer to estimate Sh_D. However, such an estimate can have errors as large as 30% if the effects of the temperature and humidity conditions of the air (H^*) and the resulting Ra_D are not accounted for. The turbulent flow experiments presented in this paper compare well with similar experiments in the literature [8,9]. The experimental data in this paper expand the data in the literature for different operating conditions (H^*), Ra_D as well as larger values of X^*.

Acknowledgement

The authors gratefully acknowledge the University of Saskatchewan, CFI and NSERC SRO for the financial support of the present study.

References

[1] S.O. Olutimayin, C.J. Simonson, Measuring and modeling vapor boundary layer growth during transient diffusion heat and moisture transfer in cellulose insulation, Int. J. Heat Mass Transfer 48 (2005) 3319–3330.

[2] F.O. Osanyintola, C.R. Iskra, C.J. Simonson, T. Ojanen, J.Ahonen, Moisture characteristics of plywood – Part II: Moisture buffering capacity of plywood interior sheathing, in: Proc. of the Nordic Building Physics Conf., Reykjavík, Iceland, June 13–15, 2005, pp. 8.

[3] L.Z. Zhang, J.L. Niu, Laminar fluid flow and mass transfer in a standard field and laboratory emission cell, Int. J. Heat Mass Transfer 46 (2003) 91–100.

[4] L.Z. Zhang, Investigation of moisture transfer effectiveness through a hydrophilic polymer membrane with a field and laboratory emission cell, Int. J. Heat Mass Transfer 49 (2006) 1176–1184.

[5] Y. Xia, A.M. Jacobi, Air-side data interpretation and performance analysis for heat exchangers with simultaneous heat and mass transfer: Wet and frosted surfaces, Int. J. Heat Mass Transfer 48 (2005) 5089–5102.

[6] H. Sadek, A.J. Robinson, J.S. Cotton, C.Y. Ching, M. Shoukri, Electrohydrodynamic enhancement of in-tube convective condensation heat transfer, Int. J. Heat Mass Transfer 49 (2006) 1647–1657.

[7] R. Yun, Y. Kim, M.S. Kim, Convective boiling heat transfer characteristics of CO_2 in microchannels, Int. J. Heat Mass Transfer 48 (2005) 235–242.

[8] W. Chuck, E.M. Sparrow, Evaporative mass transfer in turbulent forced convection duct flows, Int. J. Heat Mass Transfer 30 (2) (1987) 215–222.

[9] W. Chuck, Evaporation of water from a recessed surface to a parallel forced convection airflow, Ph.D. thesis, Department of Mechanical Engineering, University of Minnesota, Minneapolis, MN, 1985.

[10] A.T. Prata, E.M. Sparrow, Evaporation of water from a partially filled cylindrical container to a forced convection air flow, Int. J. Heat Mass Transfer 29 (4) (1986) 539–547.

[11] M.T. Pauken, An experimental investigation of combined turbulent free and forced evaporation, Exp. Therm. Fluid Sci. 18 (1999) 334–340.

[12] E.M. Sparrow, G.K. Kratz, M.J. Schuerger, Evaporation of water from a horizontal surface by natural convection, J. Heat Transfer, Trans. ASME 105 (3) (1983) 469–475.

[13] C.C. Huang, W.M. Yan, J.H. Jang, Laminar mixed convection heat and mass transfer in vertical rectangular ducts with film evaporation and condensation, Int. J. Heat Mass Transfer 48 (2005) 1772–1784.

[14] J.H. Jang, W.M. Yan, C.C. Huang, Mixed convection heat transfer enhancement through film evaporation in inclined square ducts, Int. J. Heat Mass Transfer 48 (2005) 2117–2125.

[15] J.N. Lin, P.Y. Tzeng, F.C. Chou, W.M. Yan, Convective instability of heat and mass transfer for laminar forced convection in the thermal entrance region of horizontal rectangular channels, Int. J. Heat Fluid Flow 13 (3) (1992) 250–258.

[16] R.W. Lyczkowski, C.W. Solbrig, D. Gidaspow, Forced convection heat transfer in rectangular ducts – General case of wall resistance and peripheral conduction for ventilation cooling of nuclear waste repositories, Nucl. Eng. Des. 67 (3) (1981) 357–378.

[17] R.K. Shah, A.L. London, Laminar Flow Forced Convection in Ducts, Academic Press, New York, 1978 (Ch. VII).

[18] F.O. Osanyintola, Transient moisture characteristics of spruce plywood, M.Sc. thesis, Department of Mechanical Engineering, University of Saskatchewan, Saskatoon, SK, Canada, 2005, <http://library.usask.ca/theses/available/etd-12222005-082100>.

[19] S.O. Olutimayin, Vapor boundary layer growth during transient heat and moisture transfer in cellulose insulation, M.Sc. thesis, Department of Mechanical Engineering, University of Saskatchewan, Saskatoon, SK, Canada, 2004.

[20] A. Kondjoyan, J.D. Daudin, Determination of transfer coefficients by psychrometry, Int. J. Heat Mass Transfer 36 (7) (1993) 1807–1818.

[21] Y.X. Tao, R.W. Besant, K.S. Rezkallah, A mathematical model for predicting the densification and growth of frost on a flat plate, Int. J. Heat Mass Transfer 36 (2) (1993) 353–363.

[22] ASHRAE, Fundamentals Handbook 2005, ASHRAE, Atlanta.

[23] ISO, Measurement of fluid flow by means of pressure differential devices, ISO 5167-1, Switzerland, 1991.

[24] ANSI/ASME PTC 19.1 – 1998, Test Uncertainty, ASME, New York.

[25] A. Wexler, W.A. Wildhack, Humidity and Moisture: Measurement and Control in Science and Industry, Vol. 3, Reinhold, New York, 1965, pp. 257–272.

[26] F.M. White, Fluid Mechanics, fourth ed., McGraw-Hill, Boston, 1999, pp. 771.

[27] C.J. Simonson, R.W. Besant, Energy wheel effectiveness: Part I – Development of dimensionless groups, Int. J. Heat Mass Transfer 42 (12) (1999) 2161–2170.

[28] L.Z. Zhang, J.L. Niu, Effectiveness correlations for heat and moisture transfer processes in an enthalpy exchanger with membrane cores, J. Heat Transfer-Trans. ASME 124 (5) (2002) 922–929.

[29] C.J. Simonson, R.W. Besant, Energy wheel effectiveness: Part II – Correlations, Int. J. Heat Mass Transfer 42 (12) (1999) 2171–2185.

[30] F.P. Incropera, D.P. Dewitt, Fundamentals of Heat and Mass Transfer, fifth ed., John Wiley and Sons, New York, 2002, pp. 465–531.

[31] J.-W. Ou, K.C. Cheng, R.-C. Lin, Natural convection effects on Graetz problem in horizontal rectangular channels with uniform wall temperature for large Pr, Int. J. Heat Mass Transfer 17 (1974) 835–843.

[32] T. Basak, S. Roy, T. Paul, I. Pop, Natural convection in a square cavity filled with a porous medium: Effects of various thermal boundary conditions, Int. J. Heat Mass Transfer 49 (2006) 1430–1441.

[33] W.-M. Yan, Combined buoyancy effects of thermal and mass diffusion on laminar forced convection in horizontal rectangular ducts, Int. J. Heat Mass Transfer 39 (1996) 1479–1488.

[34] R.B. Bird, W.E. Stewart, E.N. Lightfoot, Transport Phenomena, John Wiley and Sons, New York, 1960, pp. 652–663.